J Mater Sci (2017) 52:8016–8026

Shape and structural effects of R5-templated Pd nanomaterials as potent catalyst for oxygen electroreduction in alkaline media

Hongyu Yang[1], Chengwei Wen[2], Zhenghua Tang[1,3,*], Likai Wang[1], Qiannan Wang[1], Wei Yan[1], Wen Wu[1], and Shaowei Chen[1,4,*]

[1] *Guangzhou Key Laboratory for Surface Chemistry of Energy Materials, New Energy Research Institute, School of Environment and Energy, South China University of Technology, Guangzhou Higher Education Mega Centre, Guangzhou 510006, China*
[2] *Institute of Nuclear Physics and Chemistry, CAEP, P. O. Box 919-217, Mianyang 621900, Sichuan, China*
[3] *Guangdong Provincial Key Laboratory of Atmospheric Environment and Pollution Control, Guangdong Provincial Engineering and Technology Research Center for Environmental Risk Prevention and Emergency Disposal, South China University of Technology, Guangzhou Higher Education Mega Centre, Guangzhou 510006, China*
[4] *Department of Chemistry and Biochemistry, University of California, 1156 High Street, Santa Cruz, CA 95064, USA*

Received: 12 January 2017
Accepted: 13 March 2017
Published online: 20 March 2017

ABSTRACT

Bio-inspired metal nanomaterials are receiving increasing research attentions in catalytic field recently, while peptide-based method represents new revenues to fabricate stable and reactive catalyst under mild and environmental friendly conditions. Among all kinds of noble metals, peptide-based palladium nanomaterials have demonstrated excellent catalytic capabilities in a variety of organic reactions. However, their electrocatalytic properties have not been systematically studied. Herein, R5-templated Pd nanomaterials have been fabricated and employed as potent catalysts for oxygen reduction reaction (ORR). The shape and morphology of these Pd nanomaterials were manipulated by tuning the metal-to-R5 ratio. The as-prepared Pd nanomaterials demonstrated excellent ORR activity in alkaline media. R5-Pd-90 exhibited the best activity which is superior than commercial Pt/C, in terms of onset potential, diffusion-limited current density as well as long-term stability. The correlation between the shape and/or morphology of the peptide-templated Pd nanomaterials and their ORR activity has been successfully established.

Address correspondence to E-mail: zhht@scut.edu.cn; shaowei@ucsc.edu

DOI 10.1007/s10853-017-1004-y

Introduction

Noble metal nanomaterials have been attracting continuous research attentions in the past decades, mainly thanks to their versatile applications in optics and/or electronics [1, 2], probes and/or sensors [3], diagnostic and/or therapeutic agents [3, 4] as well as catalysts [5, 6]. In catalytic regime, previous studies have demonstrated that the catalytic activity of these metal nanomaterials is highly dependent on their size, shape, composition as well as subtle atomic arrangement on the nanoparticle surface. To this end, various structures have been fabricated to maximally realize their catalytic potentials. One key issue is the choice of the surface ligand, on the one hand, the ligands can passivate the metal surface to prevent bulk aggregation and stabilize the nanoparticle, while on the other hand, the binding of the ligands to metal surface can block the access of the substrate and hence significantly diminish the reactivity. Among all kinds of ligands or surface stabilizers employed, peptide has become a promising choice [7, 8]. By employing peptide, desirable physiochemical properties can be achieved by rational sequence design. Peptide-based metal nanomaterials are generally synthesized at room temperature with water as solvent, which totally avoid the harsh energy-intensive reaction conditions employed in conventional methods [8, 9]. Moreover, the inherent specific biological recognition property as well as versatile biological functionalities of the peptide sequence can be imposed onto the metal nanomaterials.

Meanwhile, palladium is a marvelous metal in the catalytic field, as it can catalyze a variety of reactions in commercial devices and industrial processes [10, 11]. Compared with gold or platinum, palladium is much cheaper with higher earth abundance. Pd nanoparticles (NPs) have demonstrated remarkable catalytic reactivity toward various reactions, and these reactions include C–C coupling reaction [12–14], 4-nitrophenol reduction [15], olefin hydrogenation [16, 17], oxidation of alcohol [18] as well as electrochemical reactions such as oxygen reduction reaction (ORR) [19–24]. To generate stable and reactive Pd nanocatalysts, a variety of templating agents including dendrimer [25], polymer [26], surfactant [27] as well as peptide [8, 28] have been employed. It has been documented that Pd^{2+} or Pd^{4+} ions can be sequestered in peptide scaffold, and upon reduction, Pd nanomaterials with controlled shape/morphology are formed [7]. Recently, our group reported the fabrication of a series of peptide-capped palladium nanoparticles, and strong surface effects were observed between peptide sequence and oxygen electroreduction activity [29].

Peptide sequence R5 (SSKKSGSYSGSKGSKRRIL) was first isolated through a phage display technique from protein silaffin. Note that, the C-terminal RRIL motif of R5 can direct the nucleation growth and form aggregates or other characteristic structures [30]. Thanks to this self-assembly property, R5 has been successfully employed to regulate the formation of several nanostructures such as silica [31], titanium phosphate [32] and titanium oxide [33]. By employing R5 as the templating agent, Bhandri et al. successfully prepared Pd nanomaterials with different shapes and morphologies, and such Pd nanomaterials demonstrated remarkably high catalytic activity for stille C–C coupling reaction and the reduction of 4-nitrophenol [15]. In addition, they fabricated Pt and Au nanomaterials templated by R5 and proved that both of them are versatile and efficient catalysts for olefin hydrogenation and 4-nitrophenol reduction [34].

Even if significant advances have been achieved for R5-templated noble metal nanomaterials as catalyst upon various organic reactions, however, their electrocatalytic capability is still unknown. For instance, do R5-templated Pd nanomaterials possess ORR activity? It is worth noting that, ORR is a key reaction which determines the efficiency of metal–air batteries and fuel cells [35–38], both of which have been well recognized to store cost-effective and environmental friendly energy devices to resolve the global energy crisis and associated severe environmental issues such as ubiquitous air pollution. The following question should be, as R5 can direct the morphology of the as-formed Pd nanomaterials, how the shape affects the ORR activity? Furthermore, can we eventually establish a correlation between the shape and morphology of R5-templated Pd nanomaterials with their electrocatalytic activity? All the above questions actually form the aim and motivation of our current study.

Herein, R5-templated Pd nanomaterials with different shape and morphologies were fabricated. All the as-prepared Pd nanomaterials exhibited excellent electrocatalytic activity toward ORR, and R5-Pd-90 outperformed other samples among the series. The

ORR activity of R5-Pd-90 is superior than of benchmark commercial Pt/C, within the context of onset potential, diffusion-limited current density as well as durability. Notably, R5-Pd-90 demonstrated exceedingly higher long-term stability than commercial Pt/C. The correlation between the shape and morphology of Pd nanomaterials with the ORR activity has been successfully established.

Materials and methods

Chemicals

Peptide R5 (SSKKSGSYSGSKGSKRRIL, >96%) was purchased from Top-Peptide (Shanghai, China). Potassium tetrachloropalladate (K_2PdCl_4, 98%), commercial Pt/C (20%) and sodium borohydride ($NaBH_4$, 98%) were acquired from Aladdin Industrial Corporation (Shanghai, China).

Synthesis of R5-templated Pd nanomaterials

R5-templated palladium nanomaterials were synthesized by following a modified procedure in the previous reports [15, 39]. The synthesis of R5-Pd-*X* ($X = 60$, 90, 120 and 150, *X* is the metal-to-R5 ratio) was conducted as follows: briefly, 2 mg peptide (R5) was first dissolved in 0.2 mL of deionized water in a 2-mL tube at room temperature to prepare a peptide solution. 9.86, 6.57, 4.93 and 3.94 μL peptide R5 aqueous solution (4.97 mM) was added into a 10-mL round-bottom flask. All the four kinds of solutions were diluted to 1776.72 μL. 76.28 μL of 38.54 mM K_2PdCl_4 was then added into the above four solutions separately. After the mixture was stirred at 300 rpm for 15 min, 147 μL of freshly prepared 0.1 M $NaBH_4$ solution was added rapidly where the solution turned from colorless to brown immediately. Then, the solution was kept stirring for at least 1 h. The R5-templated Pd nanomaterials were obtained.

Characterizations

UV–visible absorbance of the peptide-capped PdNPs was measured using a Shimadzu 2600/2700 UV–visible scanning spectrophotometer with a 1-cm quartz cuvette. HR-TEM images were acquired with high-resolution transmission electron microscope (JEOL-JEM-2010), where samples were prepared by dropcasting a catalyst dispersion directly onto a copper grid coated with a holey carbon film [40].

Electrochemical measurements

Electrochemical measurements were performed with a CHI 750E electrochemical workstation (CH Instruments Inc., Shanghai) and rotating disk electrode test system (Pine Instrument Company, Grove City) in a 0.1 M KOH aqueous solution at room temperature. A platinum wire and a Ag/AgCl electrode were employed as the counter electrode and reference electrode, respectively. The Ag/AgCl reference electrode was calibrated with respect to a reversible hydrogen electrode (RHE) by the formula of $E_{RHE} = E_{Ag/AgCl} + 0.966$ V in all measurement. The working electrode was a ring-disk electrode (diameter 5.61 mm) and cleaned by mechanical polishing with aqueous slurries of 0.3 μm alumina powders on a polishing microcloth. 20 μL Nafion (5 wt%, Aldrich) was diluted to 2 mL by ethanol. The samples were prepared by dropping 24.78, 25.28, 25.56 and 25.72 μL R5-Pd nanomaterials aqueous solution and 10 μL Nafion ethanol solution on the glassy carbon disk of the working electrode and dried at room temperature. The catalyst loading was 80.8 μg cm^{-2} for all the four samples.

Results and discussion

HR-TEM images of R5-templated Pd nanomaterials

R5-templated Pd nanomaterials were first prepared by following a modified procedure in the previous reports [15, 39]. The Pd-to-peptide ratio was controlled as 60, 90, 120 and 150. The sample was denoted as R5-Pd-*X*, where $X = 60$, 90, 120 and 150, respectively. Figure S1 presents the UV–visible absorbance spectra of the Pd nanomaterials. One can see that, for all the samples, exponential decay featureless absorbance was obtained, reminiscent of the well-known Pd colloids [41, 42]. The representative high-resolution transmission electron microscopic (HR-TEM) images of the as-prepared Pd nanomaterials can be found in Fig. 1. It can be seen that the shape and morphology changed drastically with the variation of palladium-to-peptide ratio. For the sample of R5-Pd-60, uniform spherical nanoparticles can

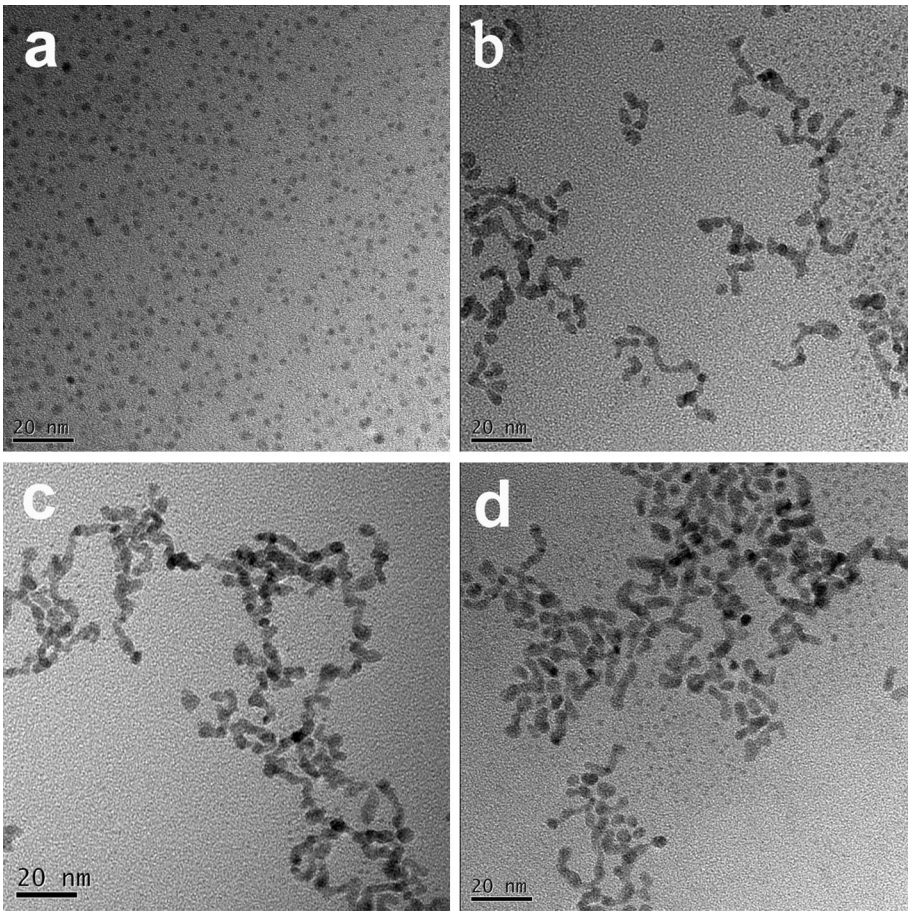

Figure 1 Representative HR-TEM images of Pd nanomaterials templated by R5 with Pd/peptide ratios of **a** 60, **b** 90, **c** 120 and **d** 150. The corresponding size distribution *histogram* of R5-Pd-60 is included in Fig. S2.

be easily identified, and the average core diameter is determined as 1.7 ± 0.4 nm (Fig. S2). For the sample of R5-Pd-90, spherical nanoparticles disappeared and nanoribbons dominated the sample. The continuous increasing of metal loading will lead to the formation of nanoparticle networks, which can be observed in both R5-Pd-120 and R5-Pd-150 samples. Nanoribbons and nanoparticle networks both exist in the sample of R5-Pd-120, while most of the particles formed networks in the sample of R5-Pd-150, and barely individual ribbon can be found.

Such morphology change with the metal-to-peptide ratio can be attributed to the self-assembly properties of the R5 sequence. Note that the RRIL motif on the C-terminal can drive the sequence to form characteristic scaffold or matrix, and upon the addition of the reducing agent, Pd nanomaterials were formed within such scaffold [7]. However, the average distance between the individual particles varies with the change of the Pd loading. With lower Pd-to-R5 ratios, the interparticle distance is quite large, which makes the particles well dispersed and not aggregated, as shown in the samples of R5-Pd-60 and R5-Pd-90. With higher Pd-to-R5 ratios, small interparticle distance was generated, which results in the linear aggregation or assembly of the particles. Such aggregation or assembly eventually led to the formation of nanoribbons or nanoparticle networks, as illustrated in the samples of R5-Pd-120 and R5-Pd-150.

Cyclic voltammograms of R5-templated Pd nanomaterials

Next, the samples were subjected for the catalytic activity tests toward ORR. Interestingly, all the R5-Pd-*X* samples demonstrated excellent ORR activity. As shown in Fig. 2a, a sharp cathodic peak at ~0.88 V from oxygen reduction can be easily indentified in the cyclic voltammograms of a glassy carbon electrode modified with each sample in O_2-saturated 0.1 M KOH solution. The cathodic peak potential is estimated as 0.87 V for R5-Pd-60, 0.88 V for R5-Pd-90, 0.88 V for R5-Pd-120 and 0.88 V for R5-

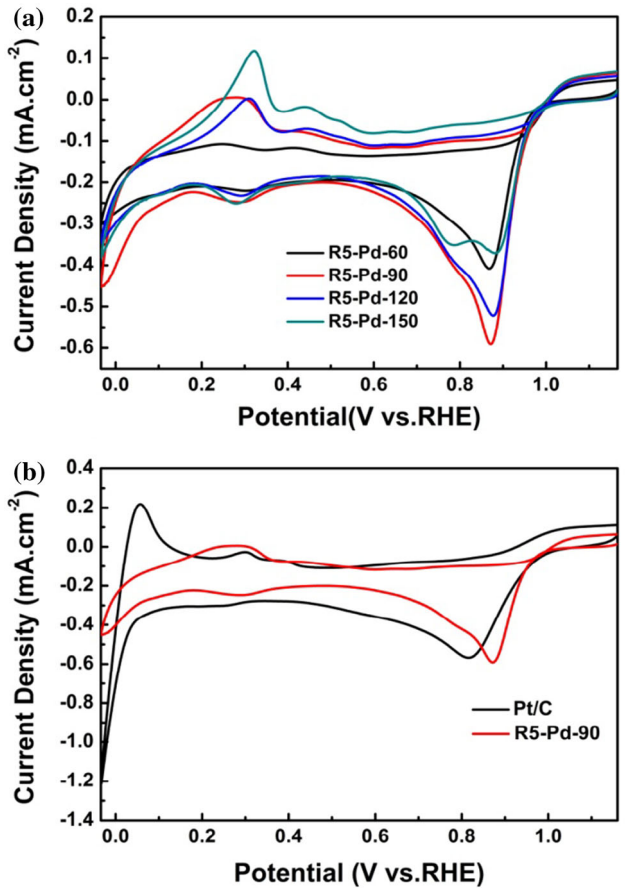

Figure 2 **a** Cyclic voltammograms of a glassy carbon electrode modified with R5-Pd-*X* samples in O_2-saturated 0.1 M KOH solution; **b** The CV comparison of R5-Pd-90 and Pt/C. Potential scan rate is 10 mV s^{-1}.

Pd-150. Such value is quite close; however, the cathodic peak current density is different for each sample. R5-Pd-90 exhibited the highest value of 0.59 mA/cm^2, slightly larger than other samples in the series. The results indicate that R5-Pd-90 might possess the best activity among the series. The ORR activity of R5-Pd-90 was further compared with commercial Pt/C, and Fig. 2b shows the cyclic voltammograms of R5-Pd-90 and Pt/C. Interestingly, R5-Pd-90 exhibited much more positive cathodic peak potential (0.88 V) than Pt/C (0.82 V), and the cathodic peak current density of R5-Pd-90 is also larger than that of Pt/C (0.59 mA/cm^2 for R5-Pd-90 vs. 0.57 mA/cm^2 for Pt/C). The above findings indicate that R5-Pd-90 probably possesses superior ORR activity than commercial Pt/C.

RRDE measurements of R5-templated Pd nanomaterials

To further probe the shape effects of the Pd nanomaterials upon ORR, we next conducted rotating ring-disk electrode (RRDE) voltammetric measurements. Table 1 summarizes all the ORR activity of the R5-Pd-*X* series and Pt/C as a comparison. As depicted in Fig. 3a, all the samples exhibited similarly high onset potential of ~0.98–0.99 V, which is higher than commercial Pt/C catalyst whose onset potential is 0.97 V. In addition, the diffusion-limited current density (at +0.50 V and 2500 rpm) was estimated to be 4.84 ± 0.21 mA/cm^2 for R5-Pd-60, 5.01 ± 0.23 mA/cm^2 for R5-Pd-90, 4.80 ± 0.12 mA/cm^2 for R5-Pd-120 and 4.25 ± 0.21 mA/cm^2 for R5-Pd-150 (Table 1). The results agree well with the above findings, as the R5-Pd-90 exhibited the best activity among the series. Once again, as illustrated in Fig. 3b, the ORR activity of R5-Pd-90 is confirmed to be superior than of Pt/C, as more positive onset potential (0.99 vs. 0.97 V) and much larger diffusion-limited current density (5.01 vs. 4.82 mA/cm^2) were acquired.

Linear scanning voltammogram (LSV) of the R5-templated Pd nanomaterials with different rotation

Table 1 Summary of Pd nanomaterials templated with R5 and Pt/C including shape, cathodic peak potential (E_p), onset potential (E_{onset}), diffusion-limited current density (j) at 0.50 V and mass activity (MA) at 0.90 V with corresponding metals

Samples	Shape	E_p (V)	E_{onset} (V)	j (mA/cm^2) at 0.50 V	Mass activity at 0.9 V (A/g)
R5-Pd-60	Spherical particles	0.87 ± 0.013	0.98 ± 0.004	−4.84 ± 0.21	44.69 ± 0.44
R5-Pd-90	Nanoribbons	0.88 ± 0.005	0.99 ± 0.003	−5.01 ± 0.23	55.70 ± 0.18
R5-Pd-120	Nanoribbons and nanoparticle networks	0.88 ± 0.002	0.98 ± 0.007	−4.80 ± 0.12	54.48 ± 0.08
R5-Pd-150	Nanoparticle networks	0.88 ± 0.005	0.98 ± 0.006	−4.25 ± 0.21	34.44 ± 0.99
Pt/C	–	0.82 ± 0.004	0.97 ± 0.007	−4.82 ± 0.25	23.18 ± 0.23

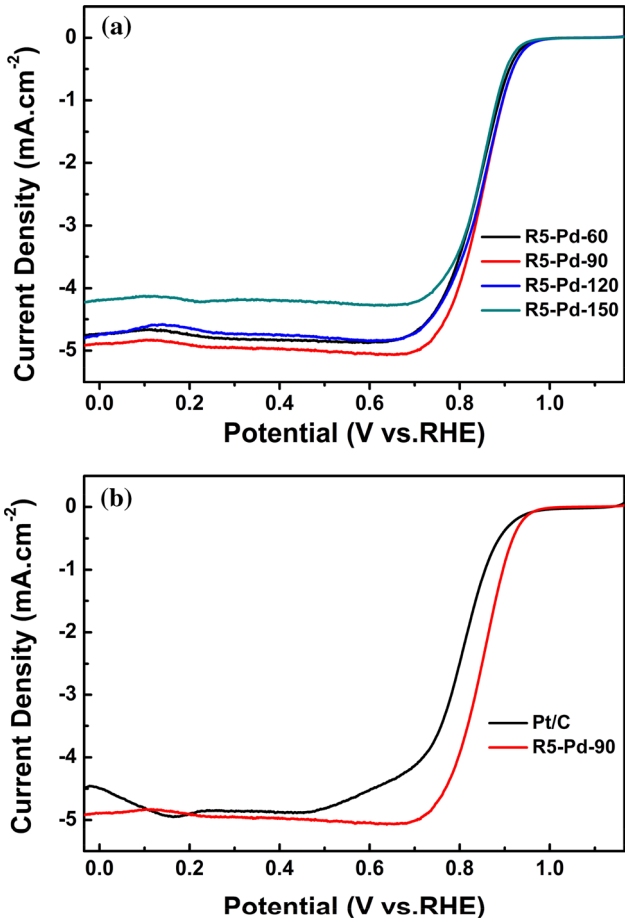

Figure 3 **a** ORR polarization curves of a glassy carbon electrode modified with the peptide R5-templated Pd nanomaterials in O_2-saturated 0.1 M KOH at 2500 rpm. **b** ORR polarization curves of R5-Pd-90 and Pt/C at 2500 rpm.

rates can be found in Fig. S3. Clearly, the voltammetric currents density increased with the increasing of electrode rotation rate. Figure S4 presents the Koutecky–Levich (K–L) plots of the R5-Pd-*X* series. In the potential range of +0.60 to +0.81 V, good linearity was exhibited and all the K–L plots possessed a consistent slope, implying that the reaction followed a first-order kinetics with respect to the oxygen concentration in the solution. The corresponding Tafel plots of R5-Pd-*X* samples and Pt/C can be found in Fig. S5. The calculated Tafel slope is 53 mV/dec for R5-Pd-60, 68 mV/dec for R5-Pd-90, 71 mV/dec for R5-Pd-120 and 55 mV/dec for R5-Pd-150, all of which is close with that of commercial Pt/C catalyst (64 mV/dec), suggesting a similar catalytic mechanism, where the first electron transfer to oxygen molecule is probably the rate determining step in the catalytic process for both the R5-Pd-*X* samples and the Pt/C catalyst [43]. Note that similar Tafel slope values have been reported in alkaline solutions for Pd nanoparticles and nanostructured Pd electrodes [20, 44].

Numbers of electron transfer and H_2O_2 yields of R5-templated Pd nanomaterials

Based on the RRDE measurements (Fig. 3), the number of electron transfer (n) and H_2O_2 yield in ORR (Fig. 4) can be quantified by

$$n = \frac{4I_d}{I_d + I_r/N} \quad (1)$$

and

$$H_2O_2\% = \frac{200I_r/N}{I_r/N + I_d} \quad (2)$$

where I_d is disk current density, I_r is ring current density and N is RRDE collection efficiency with a value of 0.37. Within the potential range of −0.03 to +0.7 V, the numbers of electron transfer (n) are 3.92–3.95 for R5-Pd-60, 3.94–3.96 for R5-Pd-90, 3.90–3.95 for R5-Pd-120, 3.89–3.95 for R5-Pd-150 and 3.86–3.95 for Pt/C catalyst. All the electron transfer numbers are quite close to 4, suggesting that a rather complete reduction from oxygen molecule to water occurred and negligible amount of H_2O_2 was produced. Obviously, R5-Pd-90 possessed the highest electron transfer number. Consistent results were further obtained in the calculated H_2O_2 yields. The

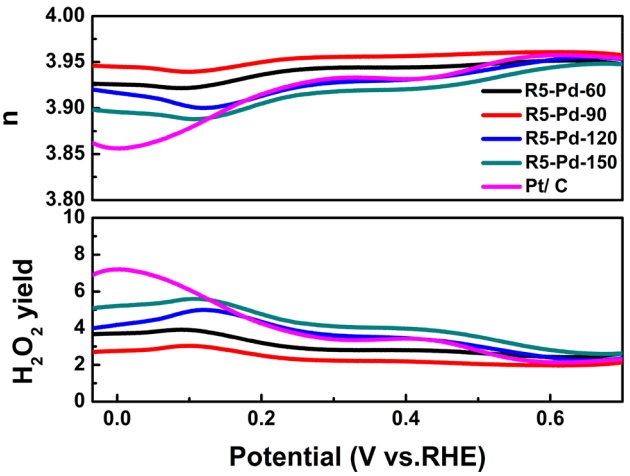

Figure 4 Number of electron transfer and plots of H_2O_2 yield and of a glassy carbon electrode modified with R5-Pd-*X* and Pt/C catalyst at 2500 rpm in O_2-saturated 0.1 M KOH solution.

H_2O_2 yields for all the R5-Pd-*X* samples nanomaterials were less than 6%, which are comparable with that of Pt/C. It is worth noting that, as exhibited in Fig. 4, R5-Pd-90 possessed an incredibly low H_2O_2 yield, as a ~3% value remained from −0.03 to 0.7 V.

The electron transfer kinetics can be further analyzed by using the Koutecky–Levich (K–L) approach [45–47]. As the voltammetric disk current (J_D) includes both kinetic (I_k) and diffusion-controlled (I_d) contributions, the K–L equation can be expressed as shown in Eqs. (3)–(5):

$$\frac{1}{J_D} = \frac{1}{I_k} + \frac{1}{I_d} = \frac{1}{I_k} + \frac{1}{B\omega^{1/2}} \tag{3}$$

$$B = 0.62nFAC_0D_0^{2/3}v^{-1/6} \tag{4}$$

$$I_k = nAFkC_0 \tag{5}$$

where ω is the electrode rotation rate, n is electron transfer number, F is the Faraday constant (96485 C mol^{-1}), A is the geometric surface area of the electrode, C_0 is the oxygen concentration in O_2-saturated solutions (1.26×10^{-6} mol cm^{-3}), D_0 is the diffusion coefficient of O_2 in 0.1 M KOH aqueous solution (1.93×10^{-5} cm^2 s^{-1}), v is the solution kinematic viscosity (1.009×10^{-2} cm^2 s^{-1}) and k is the electron transfer rate constant. As shown in Fig. S4, J_D^{-1} and $\omega^{-1/2}$ exhibited excellent linearity with very consistent slope for each sample, indicating a first-order reaction with respect to oxygen concentration. Through Eq. (4), corresponding electron transfer numbers are calculated as 3.92, 3.96, 3.93 and 3.91 (Table S1) for R5-Pd-60, R5-Pd-90, R5-Pd-120 and R5-Pd-150, respectively. As shown in Table S1, such numbers were either close or in the range of the numbers obtained from RRDE measurements.

Durability comparison of the R5-Pd-90 sample and commercial Pt/C

Lastly, the stability and durability of R5-Pd-90 sample were evaluated and compared with commercial Pt/C catalyst by chronoamperometric measurements. As illustrated in Fig. 5a, after continuous operation of 30000 s, cathodic current density of R5-Pd-90 displayed a loss of only 14.97%, while for commercial Pt/C catalyst, the loss is about 34.04%. R5-Pd-90 exhibited remarkably higher long-term durability than commercial Pt/C catalyst. To further evaluate the durability of the catalyst, accelerated durability tests were performed by cycling the catalyst over the potential range from 0 to 1.166 V at 10 mV s^{-1} in an oxygen-saturated 0.1 M KOH solution [48, 49]. As shown in Fig. 5b, the half-wave potential on commercial Pt/C shifted negatively by 22 mV after 5000 cycles test, while R5-Pd-90 displayed a smaller negative shift of only 17 mV (Fig. 5c), further attested higher durability of R5-Pd-90 than of commercial Pt/C.

ECSA tests and shape effects elucidation

To unravel how the shape and/or morphology affect the ORR activity, we conducted the electrochemically active surface area (ECSA) test of the R5-Pd-*X* samples [20]. The ECSA (m^2/g_{Pd}) of the catalysts is estimated according to the equation of ECSA = $Q_H/(A \times W_{Pd})$ [50], where Q_H is the total charge (μC), A is the charge density of Pd, which has been reported to be 424 μC/cm^2 [51], and W_{Pd} represents the Pd loading on the electrode. According to the cyclic voltammograms in Fig. S6, the ECSA value was

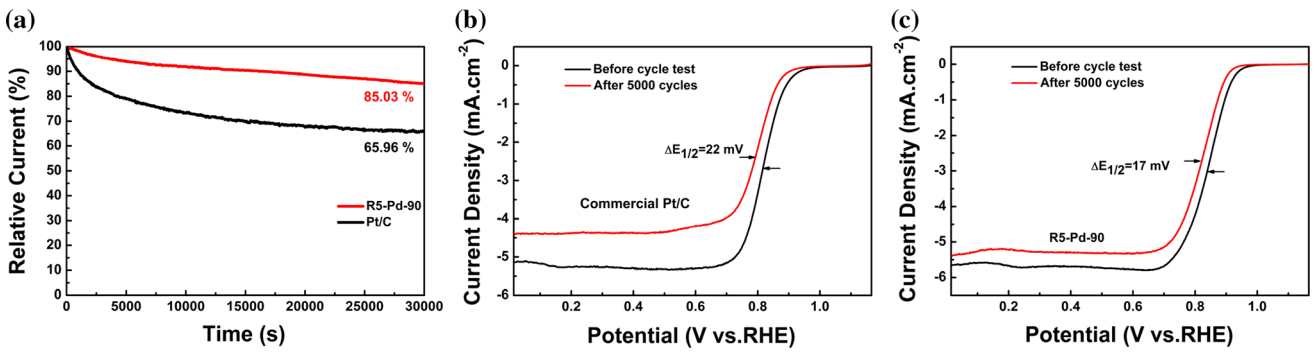

Figure 5 **a** Chronoamperometric responses for ORR at R5-Pd-90 and Pt/C electrodes in an O_2-saturated 0.1 M KOH solution at +0.5 V and 900 rpm for 30000 s. The potential scan rate is 10 mV s^{-1}. The accelerated durability tests (ADT) of commercial Pt/C (**b**) and R5-Pd-90 (**c**) were carried out before and after 5000 cycles between 0 and 1.166 V at a scan rate of 10 mV s^{-1} with a rotation speed of 2500 rpm in an O_2-saturated 0.1 M KOH solution.

determined. Note that the palladium mass loading is 3.87 μg for R5-Pd-60, 3.96 μg for R5-Pd-90, 4.00 μg for R5-Pd-120 and 4.02 μg for R5-Pd-150. The ECSA value is calculated as 24.70 m^2/g for R5-Pd-60, 28.50 m^2/g for R5-Pd-90, 23.12 m^2/g for R5-Pd-120 and 20.75 m^2/g for R5-Pd-150. The sample of R5-Pd-90 possessed the highest ECSA value in the series. This is probably the cause for the remarkably higher ORR activity. Moreover, by normalizing the current density at 0.90 V, the mass activity (MA) with respect to corresponding metal was calculated [29, 52], as listed in Table 1 and shown in Fig. S7 as well. Interestingly, all the R5-Pd-*X* samples exhibited higher MA value than Pt/C. The R5-Pd-90 sample possessed the best MA value, and it is about 2.5 times of Pt/C.

Compared to size, shape actually plays a more important role in controlling the catalytic activity, as shape not only determines the facets, but also dictates the physiochemical properties of surface atoms at corners, edges, vertexes and planes [10]. Note that the surface atoms can significantly affect the outcome of the ORR activity [53, 54]. Multiple research groups have contributed to elucidate the shape effects of Pd nanoparticles upon ORR. In 2009, Kondo et al. systematically investigated the ORR activity of the different low-index planes and found that Pd (100) is the most active plane [55]. Zhuang group revealed that the specific activity of Pd nanorod is at least tenfolds higher than that of Pd nanoparticles [56], while Shao and Xia discovered that the ORR activity of Pd nanocubes was an order of magnitude higher than that of Pd octahedra, and their performance is comparable with commercial Pt/C [57, 58]. Such findings were further confirmed by Erikson et al. as Pd nanocubes possessed threefold ORR activity of spherical nanoparticles or bulk palladium [59, 60]. Herein, strong shape effects of Pd nanomaterials templated by R5 toward ORR were observed, as nanoribbons exhibited better catalytic activity than spherical nanoparticles or nanoparticle networks. Note that the conventional approach to acquire delicate morphological control with desirable index facets normally requires tedious preparation protocols, harsh reaction conditions as well as high-energy input. The great virtues including simple and straightforward sample preparation, environmentally friendly conditions and extremely low-energy input of the peptide-templating approach make it a promising strategy for fabricating noble metal nanomaterials with desired shape or morphology as highly efficient catalysts for electrochemical reactions.

Conclusions

In summary, R5-templated Pd nanomaterials were fabricated and employed as potent electrocatalysts for ORR. The shape and morphology of the Pd nanomaterials can be manipulated by tuning the palladium-to-R5 ratio. The as-prepared Pd nanomaterials exhibited excellent ORR activity, and R5-Pd-90 with nanoribbons is the best sample among the series. The correlation between the shape/morphology of R5-templated Pd nanomaterials and their corresponding ORR activity has been successfully established. Notably, the ORR performance of R5-Pd-90 is superior than of commercial Pt/C, as more positive onset potential, much larger diffusion-limited current density, greater mass activity as well as markedly higher long-term stability were achieved. The results might pave a pathway for the rational design of Pd nanomaterials with desirable morphology and optimized electrochemical properties for electrocatalytic reactions.

Acknowledgements

Z. H. T acknowledges financial support from the National Natural Science Foundation of China (No. 21501059), Project of Public Interest Research and Capacity Building of Guangdong Province (2015A010105009), Guangdong Natural Science Funds for Distinguished Young Scholars (No. 2015A030306006) as well as Guangdong Innovative and Entrepreneurial Research Team Program (No. 2014ZT05N200). S. W. C. thanks the National Science Foundation for partial support of the work (CHE-1265635 and DMR-1409396).

Electronic supplementary material: The online version of this article (doi:10.1007/s10853-017-1004-y) contains supplementary material, which is available to authorized users.

References

[1] Lee YJ, Lee Y, Oh D, Chen T, Ceder G, Belcher AM (2010) Biologically activated noble metal alloys at the nanoscale: for lithium ion battery anodes. Nano Lett 10:2433–2440

[2] Lee Y, Kim J, Yun DS, Nam YS, Shao-Horn Y, Belcher AM (2012) Virus-templated Au and Au–Pt core-shell nanowires and their electrocatalytic activities for fuel cell applications. Energy Environ Sci 5:8328–8334

[3] Chinen AB, Guan CM, Ferrer JR, Barnaby SN, Merkel TJ, Mirkin CA (2015) Nanoparticle probes for the detection of cancer biomarkers, cells, and tissues by fluorescence. Chem Rev 115:10530–10574

[4] Yang X, Yang M, Pang B, Vara M, Xia Y (2015) Gold nanomaterials at work in biomedicine. Chem Rev 115:10410–10488

[5] An K, Somorjai GA (2012) Size and shape control of metal nanoparticles for reaction selectivity in catalysis. ChemCatChem 4:1512–1524

[6] Li G, Jin R (2013) Atomically precise gold nanoclusters as new model catalysts. Acc Chem Res 46:1749–1758

[7] Dickerson MB, Sandhage KH, Naik RR (2008) Protein- and peptide-directed syntheses of inorganic materials. Chem Rev 108:4935–4978

[8] Chen C-L, Rosi NL (2010) Peptide-based methods for the preparation of nanostructured inorganic materials. Angew Chem Int Ed 49:1924–1942

[9] Briggs BD, Knecht MR (2012) Nanotechnology meets biology: peptide-based methods for the fabrication of functional materials. J Phys Chem Lett 3:405–418

[10] Zhang H, Jin M, Xiong Y, Lim B, Xia Y (2013) Shape-Controlled synthesis of Pd nanocrystals and their catalytic applications. Acc Chem Res 46:1783–1794

[11] MaF Akhairi, Kamarudin SK (2016) Catalysts in direct ethanol fuel cell (DEFC): an overview. Int J Hydrog Energy 41:4214–4228

[12] Coppage R, Slocik JM, Sethi M, Pacardo DB, Naik RR, Knecht MR (2010) Elucidation of peptide effects that control the activity of nanoparticles. Angew Chem Int Ed 49:3767–3770

[13] Coppage R, Slocik JM, Briggs BD, Frenkel AI, Heinz H, Naik RR, Knecht MR (2011) Crystallographic recognition controls peptide binding for bio-based nanomaterials. J Am Chem Soc 133:12346–12349

[14] Coppage R, Slocik JM, Ramezani-Dakhel H, Bedford NM, Heinz H, Naik RR, Knecht MR (2013) Exploiting localized surface binding effects to enhance the catalytic reactivity of peptide-capped nanoparticles. J Am Chem Soc 135:11048–11054

[15] Bhandari R, Knecht MR (2011) Effects of the material structure on the catalytic activity of peptide-templated Pd nanomaterials. ACS Catal 1:89–98

[16] Wilson OM, Knecht MR, Garcia-Martinez JC, Crooks RM (2006) Effect of Pd nanoparticle size on the catalytic hydrogenation of allyl alcohol. J Am Chem Soc 128:4510–4511

[17] Crespo-Quesada M, Yarulin A, Jin M, Xia Y, Kiwi-Minsker L (2011) Structure sensitivity of alkynol hydrogenation on shape- and size-controlled palladium nanocrystals: Which sites are most active and selective? J Am Chem Soc 133:12787–12794

[18] Harada T, Ikeda S, Hashimoto F, Sakata T, Ikeue K, Torimoto T, Matsumura M (2010) Catalytic activity and regeneration property of a Pd nanoparticle encapsulated in a hollow porous carbon sphere for aerobic alcohol oxidation. Langmuir 26:17720–17725

[19] Guo S, Zhang S, Sun S (2013) Tuning nanoparticle catalysis for the oxygen reduction reaction. Angew Chem Int Ed 52:8526–8544

[20] Deming CP, Mercado R, Gadiraju V, Sweeney SW, Khan M, Chen S (2015) Graphene quantum dots-supported palladium nanoparticles for efficient electrocatalytic reduction of oxygen in alkaline media. ACS Sustain Chem Eng 3:3315–3323

[21] Jiang G, Zhu H, Zhang X, Shen B, Wu L, Zhang S, Lu G, Wu Z, Sun S (2015) Core/shell face-centered tetragonal FePd/Pd nanoparticles as an efficient non-Pt catalyst for the oxygen reduction reaction. ACS Nano 9:11014–11022

[22] Zhou W, Li M, Ding OL, Chan SH, Zhang L, Xue Y (2014) Pd particle size effects on oxygen electrochemical reduction. Int J Hydrog Energy 39:6433–6442

[23] Tang Y, Chi X, Zou S, Zeng X (2016) Facet effects of palladium nanocrystals for oxygen reduction in ionic liquids and for sensing applications. Nanoscale 8:5771–5779

[24] Jukk K, Alexeyeva N, Sarapuu A, Ritslaid P, Kozlova J, Sammelselg V, Tammeveski K (2013) Electroreduction of oxygen on sputter-deposited Pd nanolayers on multi-walled carbon nanotubes. Int J Hydrog Energy 38:3614–3620

[25] Anderson RM, Yancey DF, Zhang L, Chill ST, Henkelman G, Crooks RM (2015) A theoretical and experimental approach for correlating nanoparticle structure and electrocatalytic activity. Acc Chem Res 48:1351–1357

[26] Narayanan R, El-Sayed MA (2003) Effect of catalysis on the stability of metallic nanoparticles: suzuki reaction catalyzed by PVP-palladium nanoparticles. J Am Chem Soc 125:8340–8347

[27] Naresh N, Wasim FGS, Ladewig BP, Neergat M (2013) Removal of surfactant and capping agent from Pd nanocubes (Pd-NCs) using tert-butylamine: its effect on electrochemical characteristics. J Mater Chem A 1:8553–8559

[28] Bhandari R, Coppage R, Knecht MR (2012) Mimicking nature's strategies for the design of nanocatalysts. Catal Sci Technol 2:256–266

[29] Yang H, Tang Z, Yan W, Wang L, Wang Q, Zhang Y, Liu Z, Chen S (2017) Peptide capped Pd nanoparticles for oxygen electroreduction: strong surface effects. J Alloys Compd 702:146–152

[30] Knecht MR, Wright DW (2003) Functional analysis of the biomimetic silica precipitating activity of the R5 peptide from Cylindrotheca fusiformis. Chem Commun (24): 3038–3039

[31] Sewell SL, Wright DW (2006) Biomimetic synthesis of titanium dioxide utilizing the R5 peptide derived from cylindrotheca fusiformis. Chem Mater 18:3108–3113

[32] Cole KE, Ortiz AN, Schoonen MA, Valentine AM (2006) Peptide- and long-chain polyamine- induced synthesis of micro- and nanostructured titanium phosphate and protein encapsulation. Chem Mater 18:4592–4599

[33] Naik RR, Whitlock PW, Rodriguez F, Brott LL, Glawe DD, Clarson SJ, Stone MO (2003) Controlled formation of biosilica structures in vitro. Chem Commun (2):238–239

[34] Bhandari R, Knecht MR (2012) Synthesis, characterization, and catalytic application of networked au nanostructures fabricated using peptide templates. Catal Sci Technol 2:1360–1366

[35] Debe MK (2012) Electrocatalyst approaches and challenges for automotive fuel cells. Nature 486:43–51

[36] Kraytsberg A, Ein-Eli Y (2014) Review of advanced materials for proton exchange membrane fuel cells. Energy Fuels 28:7303–7330

[37] Winter M, Brodd RJ (2004) What are batteries, fuel cells, and supercapacitors? Chem Rev 104:4245–4270

[38] Peighambardoust SJ, Rowshanzamir S, Amjadi M (2010) Review of the proton exchange membranes for fuel cell applications. Int J Hydrog Energy 35:9349–9384

[39] Bhandari R, Pacardo DB, Bedford NM, Naik RR, Knecht MR (2013) Structural control and catalytic reactivity of peptide-templated Pd and Pt nanomaterials for olefin hydrogenation. J Phys Chem C 117:18053–18062

[40] Gu H, Ma C, Gu J, Guo J, Yan X, Huang J, Zhang Q, Guo Z (2016) An overview of multifunctional epoxy nanocomposites. J Mater Chem C 4:5890–5906

[41] Creighton JA, Eadon DG (1991) Ultraviolet-visible absorption spectra of the colloidal metallic elements. J Chem Soc, Faraday Trans 87:3881–3891

[42] Coppage R, Slocik JM, Briggs BD, Frenkel AI, Naik RR, Knecht MR (2012) Determining peptide sequence effects that control the size, structure, and function of nanoparticles. ACS Nano 6:1625–1636

[43] He G, Song Y, Liu K, Walter A, Chen S, Chen S (2013) Oxygen reduction catalyzed by platinum nanoparticles supported on graphene quantum dots. ACS Catal 3:831–838

[44] Alexeyeva N, Sarapuu A, Tammeveski K, Vidal-Iglesias FJ, Solla-Gullón J, Feliu JM (2011) Electroreduction of oxygen on Vulcan carbon supported Pd nanoparticles and Pd–M nanoalloys in acid and alkaline solutions. Electrochim Acta 56:6702–6708

[45] Deming CP, Zhao A, Song Y, Liu K, Khan MM, Yates VM, Chen S (2015) Alkyne-protected AuPd alloy nanoparticles for electrocatalytic reduction of oxygen. ChemElectroChem 2:1719–1727

[46] Wang Q, Tang Z, Wang L, Yang H, Yan W, Chen S (2016) Morphology control and electro catalytic activity towards oxygen reduction of peptide-templated metal nanomaterials: a comparison between Au and Pt. ChemistrySelect 1:6044–6052

[47] Yan W, Tang Z, Wang L, Wang Q, Yang H, Chen S (2017) PdAu alloyed clusters supported by carbon nanosheets as efficient electrocatalysts for oxygen reduction. Int J Hydrog Energy 42:218–227

[48] Zadick A, Dubau L, Demirci UB, Chatenet M (2016) Effects of Pd nanoparticle size and solution reducer strength on Pd/C electrocatalyst stability in alkaline electrolyte. J Electrochem Soc 163:F781–F787

[49] Wang L, Tang Z, Yan W, Wang Q, Yang H, Chen S (2017) Co@Pt Core@Shell nanoparticles encapsulated in porous carbon derived from zeolitic imidazolate framework 67 for oxygen electroreduction in alkaline media. J Power Sources 343:458–466

[50] Ding L-X, Wang A-L, Li G-R, Liu Z-Q, Zhao W-X, Su C-Y, Tong Y-X (2012) Porous Pt–Ni–P composite nanotube arrays: highly electroactive and durable catalysts for methanol electrooxidation. J Am Chem Soc 134:5730–5733

[51] Zhou Z-Y, Kang X, Song Y, Chen S (2011) Butylphenyl-functionalized palladium nanoparticles as effective catalysts for the electrooxidation of formic acid. Chem Commun 47:6075–6077

[52] Zhang X, Xiao Q, Zhang Y, Jiang X, Yang Z, Xue Y, Yan Y-M, Sun K (2014) La_2O_3 doped carbonaceous microspheres: a novel bifunctional electrocatalyst for oxygen reduction and evolution reactions with ultrahigh mass activity. J Phys Chem C 118:20229–20237

[53] Tang W, Lin H, Kleiman-Shwarsctein A, Stucky GD, Mcfarland EW (2008) Size-dependent activity of gold nanoparticles for oxygen electroreduction in alkaline electrolyte. J Phys Chem C 112:10515–10519

[54] Chen W, Chen S (2009) Oxygen electroreduction catalyzed by gold nanoclusters: strong core size effects. Angew Chem Int Ed 48:4386–4389

[55] Kondo S, Nakamura M, Maki N, Hoshi N (2009) Active sites for the oxygen reduction reaction on the low and high

index planes of palladium. J Phys Chem C 113:12625–12628

[56] Xiao L, Zhuang L, Liu Y, Lu J, Abruña HD (2009) Activating Pd by morphology tailoring for oxygen reduction. J Am Chem Soc 131:602–608

[57] Shao M, Yu T, Odell JH, Jin M, Xia Y (2011) Structural dependence of oxygen reduction reaction on palladium nanocrystals. Chem Commun 47:6566–6568

[58] Shao M, Odell J, Humbert M, Yu T, Xia Y (2013) Electrocatalysis on shape-controlled palladium nanocrystals: oxygen reduction reaction and formic acid oxidation. J Phys Chem C 117:4172–4180

[59] Erikson H, Sarapuu A, Tammeveski K, Solla-Gullón J, Feliu JM (2011) Enhanced electrocatalytic activity of cubic Pd nanoparticles towards the oxygen reduction reaction in acid media. Electrochem Commun 13:734–737

[60] Erikson H, Sarapuu A, Alexeyeva N, Tammeveski K, Solla-Gullón J, Feliu JM (2012) Electrochemical reduction of oxygen on palladium nanocubes in acid and alkaline solutions. Electrochim Acta 59:329–335